The spark-associated soliton model for pulsar radio emission

George I. Melikidze[1,2], Janusz A. Gil[1] and Avtandil D. Pataraya[2]

gogi@astro.ca.sp.zgora.pl, jag@astro.ca.sp.zgora.pl

ABSTRACT

We propose a new, self-consistent theory of coherent pulsar radio emission based on the non-stationary sparking model of Ruderman & Sutherland (1975), modified by Gil & Sendyk (2000) in the accompanying Paper I. According to these authors, the polar cap (with a radius $r_p \simeq 10^4 P^{-0.5}$ cm) is populated by about $(r_p/h)^2$ sparks of a characteristic perpendicular dimension D approximately equal to the polar gap height scale $h \sim 5 \times 10^3 P^{3/7}$ cm, separated from each other also by about h. Each spark reappears in approximately the same place on the polar cap for a time scale much longer than its 10 μs life-time and delivers to the open magnetosphere a sequence of $e^- e^+$ clouds which flow orderly along a flux tube of dipolar magnetic field lines. The overlapping of particles with different momenta from consecutive clouds leads to effective two-stream instability, which triggers electrostatic Langmuir waves at the altitudes of about 50 stellar radii. This is the only known instability which can develop at the low altitudes, where the observed pulsar radio emission originates. The electrostatic oscillations are modulationally unstable and their nonlinear evolution results in formation of "bunch-like" charged solitons. A characteristic soliton length along magnetic field lines is about 30 cm, so they are capable of emitting coherent curvature radiation at radio wavelengths. A perpendicular cross-section of each soliton at radiation altitudes follows from a dipolar spread of a plasma cloud with a characteristic dimension near the star surface of about $D \approx h \approx 50$ meters. The net soliton charge is about 10^{21} fundamental charges, contained within a volume of about 10^{14} cm^3. For a typical pulsar, there are about 10^5 solitons associated with each of about 25 sparks operating on the polar cap at any instant. One soliton moving relativisticaly along dipolar field lines with a Lorentz factor of the order of 100 generates a power of about 10^{21} erg/s by means of curvature radiation. Then the total power of a typical radio pulsar can be estimated as being about 10^{27-28} erg/s. The energy of the soliton curvature radiation is supported by kinetic energy of secondary electron-positron plasma created by the primary beam produced by the accelerating potential drop within the polar gap. A significant fraction of kinetic energy generated by sparks is radiated away in form of the observed coherent radio emission.

Subject headings: pulsar: radio emission, plasma—nonlinear waves: solitons

---

[1]J. Kepler Astronomical Center, Pedagogical University, Lubuska 2, 65-265, Zielona Góra, Poland

[2]Abastumani Astrophysical Observatory, Al.Kazbegi ave. 2a, Tbilisi 380060, Georgia

1.   Introduction

Although more than 30 years have past since the discovery of pulsars, the mechanism of their radio-emission still remains a mystery. This concerns both the fundamental problem of coherency, and the specific modulation of pulsar radiation in the form of micropulses, subpulses and characteristic stable mean profiles. Ruderman and collaborators in a series of papers (Ruderman & Sutherland 1975; Cheng & Ruderman 1977a,b, 1980) have attempted to solve for both the mechanism of coherence of single particle radiation and the organization of emitting regions. Although their two-stream plasma instability has proven inefficient in producing observable flux, the latter was partially successful in explaining details of pulsar radiation modulations. Recently, Gil & Sendyk (2000; henceforth Paper I) have modified the spark model of Ruderman & Sutherland (1975) and demonstrated that it explains naturally the single-pulse structure (including a subpulse drift), the mean profile morphology and polarization. All the observed characteristics are determined by two basic pulsar parameters: period P and its derivative $\dot{P}$, along with an observing geometry (inclination and impact angles). They argued that the pulsar polar cap is populated by a number of sparks with both characteristic dimension and distance between adjacent sparks equal approximately to the polar gap height $h \simeq 5 \times 10^3 \ P^{3/7}$ cm, where P is pulsar period in seconds. Therefore, the number of sparks on the polar cap is determined by the so-called complexity parameter $a = r_p/h$ (Paper I), where $r_p \simeq 10^4 \ P^{-0.5}$ cm is the canonical polar cap radius. Recently, Deshpande & Rankin (1999) have analyzed with unprecedented detail the driftbands of subpulses in PSR B0943+10. They were able to determine both the radiation pattern and the observing geometry corresponding to a peripheral sightline grazing the stable system of 20 spark-associated subpulse beams which rotate around the pulsar beam axis. This finding is the strongest evidence of a non-stationary sparking discharge of high potential drop in the polar cap acceleration region (polar gap) in radio pulsars (Xu et. al 1999; Paper I).

Gil & Sendyk (Paper I) argued that one spark is anchored to the local pole of a non-dipolar (presumable sun spot-like) surface magnetic field. This prevents sparks from fast motion along the planes of field lines towards the pole, which allows them to reappear in approximately the same places (modulo the slow $\mathbf{E} \times \mathbf{B}$ drift across the planes of field lines) on time scales much longer than 10 μs. If a spark reappears at least twice at one place on the polar cap, then a strong Langmuir turbulence should occur due to the two-stream instability (Usov 1987; Ursov & Usov 1988; Gil et al. 1997; Asseo & Melikidze 1998). In fact, each spark emits a sequence of e^-e^+ plasma clouds flowing orderly along a tube of spark-associated field lines, which can penetrate each other due to large spread of momenta. Such a penetration ignites an efficient two-stream like instability, generating strong Langmuir waves. In this paper we consider a nonlinear evolution of Langmuir electrostatic oscillations generated by the two-stream instability within a spark-associated plasma column and show that it leads to a soliton formation, capable of generating a 'bunch-like' coherent radiation, with the all characteristic features of the observed pulsar radio emission.

The main and the most decisive problem for coherency of curvature radiation is the formation and stability of the charged bunches. Despite many attempts there is no sufficiently well-grounded

theory for bunch formation so far. The curvature radiation of charged particle bunches, themselves produced by a linear plasma wave, has been proposed as a possible mechanism of pulsar radio emission (e.g., Ruderman & Sutherland 1975; Cheng & Ruderman 1977a). However, as pointed out by Lominadze et al. (1986), bunches produced by a linear electrostatic wave can exists only over extremely short time scale. As the wave propagates along the magnetic field line, each fixed spatial point senses the alternating electrostatic field as time elapses. After a half-period this field changes direction and it begins to 'bunch' particles of the opposite sign. It is thus necessary that the time scale of the process by which the bunches radiate must be significantly shorter than half of the plasma oscillation period. At the very least, the condition $\omega_l < \omega$ must hold (where ω_l and ω are the frequencies of the plasma waves and the waves emitted by bunches, respectively). On the other hand, for the radiation to be coherent, the linear characteristic dimension of bunches must be shorter than about half wavelength of the radiated wave. Since in the linear approximation the dimension of the bunch is determined by the half wavelength of the plasma waves, another necessary condition $k_l > k$ should be satisfied (here k_l and k are the wave vectors of Langmuir waves and curvature radiation, respectively). If the radiated wave has a 'vacuum' spectrum $\omega \approx kc$, then these conditions are incompatible with each other. Thus, the bunching associated with high frequency linear plasma oscillations cannot be responsible for the coherent pulsar radio emission (see also Melrose & Gedalin 1999). In this paper we propose a new promising model for bunch formation due to slowly-varying nonlinear plasma processes. Our model is self-consistent and free of fundamental problems mentioned above.

Asseo & Melikidze (1998) have recently studied possible instabilities in the non-stationary spark-associated magnetospheric plasma. They have found that the two-stream instability within spark-associated plasma clouds is the only one which can develop at altitudes below 10% of the light cylinder, that is at altitudes about 50 stellar radii $R = 10^6$ cm, where pulsar radio emission is expected to originate (e.g., Kijak & Gil 1997, 1998). As already stated above, Langmuir waves generated due to these instabilities can not directly produce the observed pulsar radio emission. In fact, their frequency (about 100 GHz) is much higher than the observed pulsar radio frequencies (see Asseo & Melikidze 1998; Melrose & Gedalin 1999). Moreover, having an electrostatic nature they can not escape from the plasma. However, as we will argue in this paper, they can form a charge-separated solitons. A packet of plasma waves propagating in the relativistic electron-positron plasma with phase velocities close to (but less than) the velocity of light is unstable from the modulational standpoint, and its nonlinear evolution results in the formation of a nonlinear solitary wave soliton. This process is described by the nonlinear Schrödinger equation, taking into account the nonlinear Landau damping (Melikidze & Pataraya 1980a,b, 1984). The role of the low-frequency perturbations in case of the electron-positron plasma (that is in the absence of ion sonic waves) is played by the nonlinear beatings of plasma waves and the nonlinear dumping is determined by the resonant interaction of the beatings with plasma particles. As we argue in this paper, in condition prevailing within spark-associated pulsar magnetosphere, Langmuir soliton can cause an effective charge separation for a period of time sufficiently long to provide a coherent curvature radiation responsible for the observed pulsar radio emission.

2. Coherent curvature radio emission in pulsars

2.1. Linear theory

The properties of the secondary electron-positron plasma created via Sturrock (1971) multiplication process by the primary positrons depend on the radius of curvature $\mathcal{R}$ of magnetic field lines above the gap, where the accelerating electric field is negligible. We assume that $\mathcal{R}$ is almost equal to the radius of curvature at the stellar surface $\mathcal{R}_0 \leqslant 10^6$cm (Ruderman & Sutherland 1975; Paper I). Then, Sturrock's multiplication factor $\varkappa \geqslant 10^4$ and the Lorentz factor of the secondary $e^- e^+$ plasma $\gamma_p \leqslant 100$. In fact, let us consider a canonical maximum potential drop within the gap (Sturrock 1971; Ruderman & Sutherland 1975)

$$V \sim 1.7 \times 10^{12} P^{0.36} \dot{P}_{-15}^{0.5} \qquad \text{Volts}, \tag{1}$$

which holds for $\mathcal{R}_6 = \mathcal{R}/10^6 \approx 1$, where $\dot{P}_{-15}$ is period derivative in 10^{-15}s s^{-1}. Then, the corresponding Lorentz factor of the primary particles should be $\gamma_b \approx V \left(e/m_e c^2 \right) \sim 3 \times 10^6$ and for average Lorentz factor of spark-generated plasma particles we have $\gamma_p \approx \gamma_b/(2\varkappa) \sim 10^2$. The secondary plasma with a number density $n_p \simeq \varkappa n_{GJ}$ is penetrated by the beam of primary particles with a Goldreich-Julian corotational number density (Goldreich & Julian 1969)

$$n_{GJ} \sim 5.6 \times 10^5 \left(\frac{\dot{P}_{-15}}{P} \right)^{0.5} R_{50}^{-3} \qquad \text{cm}^{-3}, \tag{2}$$

where $R_{50} = r/(50R)$ is the radial distance in units of 50 stellar radii $R = 10^6$ cm.

It is now well known that the interaction proposed by many authors (e.g., Lominadze et al. 1986; Machabeli 1991; Kazbegi et al. 1991, 1992; Lutikov et al. 1999) between the primary beam and magnetospheric plasma is too weak at low altitudes (say $r \sim 50R$), since the instability development requires that drift velocity of the primary particles becomes sufficiently high (Kazbegi et al. 1992). As we already mentioned, there is only one instability which can produce a strong initial turbulence at low altitudes. This instability is triggered by the non-stationary process of plasma creation associated with sparking discharge of the acceleration region above the polar cap. Before we start exploring the nonlinear effects, let us briefly summarize the results of the linear approach performed by Asseo & Melikidze (1998). The plasma frequency and the frequency of excited plasma waves are respectively

$$\omega_p \sim 4.2 \times 10^9 \; R_{50}^{-1.5} \varkappa_4^{0.5} \left(\frac{\dot{P}_{-15}}{P} \right)^{0.25} \qquad \text{rad s}^{-1} \tag{3}$$

and

$$\omega_l \sim 2 \, \delta_\omega \, \gamma_p \, \omega_p \sim 4.2 \times 10^{11} \; R_{50}^{-1.5} \varkappa_4^{0.5} \gamma_2^{0.5} \left(\frac{\dot{P}_{-15}}{P} \right)^{0.25} \qquad \text{rad s}^{-1}. \tag{4}$$

In these expressions, δ_ω is the parameter which has been calculated in Asseo & Melikidze (1998) and estimated as ~ 0.5, $\varkappa_4 = \varkappa/10^4$, where $\varkappa \sim \gamma_b/\gamma_p$, and $\gamma_2 = \gamma_p/100$. Here R_{50} is an altitude

of instability region, and for typical pulsars $R_{50} \sim 1$. Also $\varkappa_4$ and γ_2 are regarded as being close to unity (e.g., Ruderman & Sutherland 1975). Thus for typical values of pulsar parameters $\omega_p \sim 10^{10}$ rad s^{-1} and $\omega_l \sim 10^{12}$ rads^{-1}.

The Langmuir waves with frequency ω_l determined by equation (4) are generated by the following simple mechanism (Usov 1987; Ursov & Usov 1988; Gil et al. 1997; Asseo & Melikidze 1998). The repeatable sparking creates a succession of plasma clouds moving along a tube of magnetic field lines, each cloud containing particles with a large spread of momenta. Overlapping of particles with different energies (determined by γ_T, see Appendix C and Fig.1) from adjacent clouds ignites strong Langmuir oscillations, which may lead eventually to the generation of coherent pulsar radio emission. Interestingly, this instability is the only one which, according to our knowledge, develops at altitudes of the order of a few percent of the light cylinder radius, where the pulsar radio emission is expected to originate (Cordes 1978; Cordes 1992; Kijak & Gil 1997, 1998). The altitude R_{50} at which the two-stream instability can develop depends on the average Lorentz factor of plasma γ_p. This has been estimated by Asseo & Melikidze (1998, their Fig. 6); see also a kinematic estimate in equation (5) below. Specifically, if $\gamma_2 = 0.5$ then $R_{50} \simeq 0.1 - 0.5$; if $\gamma_2 = 0.75$ then $R_{50} \simeq 0.3 - 1.1$; if $\gamma_2 = 1$ then $R_{50} \simeq 0.5 - 2$.

The two adjacent secondary plasma clouds corresponding to the two consecutive sparks are separated by about $\Delta t \sim h/c$ (typically 10^{-7} s), where $h \simeq 5 \times 10^3 \mathcal{R}_6^{2/7} B_{12}^{-4/7} P^{3/7}$ cm is the polar gap height, $\mathcal{R}_6 = \mathcal{R}/R$ and $B_{12} = B_0/10^{12}$ (Ruderman & Sutherland 1975). Let us estimate the time ΔT after which particles with different Lorentz factors will overcome each other. The corresponding velocity difference is determined by the average Lorentz factor as $\Delta v \simeq c/(2\gamma_p^2)$. It is easy to show that $\Delta T \sim h/\Delta v \sim 2\gamma_p^2 \, h/c$. The distance covered during this time $r_{in} \sim c\Delta T \sim 2\gamma_p^2 h \sim 10^8 \gamma_2^2 \mathcal{R}_6^{2/7} B_{12}^{-4/7} P^{3/7} \gg R$, and thus one can write the expression

$$R_{50} \sim \gamma_2^2 \mathcal{R}_6^{2/7} B_{12}^{-4/7} P^{3/7}. \tag{5}$$

This kinematic estimate of the altitude of the instability region agrees roughly with estimates of the altitude of radio emission region $r/R = 50 \cdot R_{50} \sim 50 \cdot P^{0.33 \pm 0.05}$ given by Kijak & Gil (1997, 1998).

The linear growth rate Γ_l, which should satisfy the condition $\Gamma_l \gg c/\Delta r$, where $\Delta r \sim 50 \cdot R_{50} \cdot 10^6$ cm is characteristic longitudinal dimension of the instability region, can be written as

$$\Gamma_l \sim 1.1 \times 10^6 \; \gamma_2^{-1.5} \; R_{50}^{-1.5} \left(\frac{\dot{P}_{-15}}{P} \right)^{0.25}, \tag{6}$$

and the above condition for the instability development in the resulting plasma cloud is

$$\gamma_2^{-1.5} \; R_{50}^{-1.5} \left(\frac{\dot{P}_{-15}}{P} \right)^{0.25} \gg 0.1, \tag{7}$$

(Asseo & Melikidze 1998). It is obvious that for typical values of magnetospheric plasma parameters $(\gamma_2 \sim R_{50} \sim \dot{P}_{-15} \sim P \sim 1)$ the growth rate of instability is high enough to provide a strong

Langmuir turbulence, that is the condition (7) is well satisfied. In the following we will explore a nonlinear evolution of this turbulence and argue that it results in formation of a 'bunch-like' charged soliton, capable of emitting coherent curvature radiation at radio wavelengths.

2.2.   The nonlinear theory

It is obvious that the excitation of longitudinal electrostatic waves still does not explain the observed radio emission of pulsars. We need some mechanism which leads to the generation of low frequency waves capable of escaping from the pulsar magnetosphere in the form of coherent radio emission. Karpman et al. (1975) were the first to propose Langmuir solitons as a possible bunching mechanism. The net charge in their soliton was due to mass difference between protons and electrons. Melikidze & Pataraya (1980b, 1984) have studied the same problem in the more realistic case (for pulsars)of an electron-positron plasma and proposed two possible reasons for charge separation: (i) small admixture of ions, (ii) difference in the distribution functions of electrons and positrons. Such a difference occurs naturally in the case of the pulsar magnetospheric plasma, which will be discussed later in this paper. Following Melikidze & Pataraya (1984), Asseo (1993) discussed the possibility of curvature radiation of Langmuir soliton, but without a consideration of non-stationary character of electron-positron plasma. The basic soliton parameters like dimensions, volume and net charge are markedly different in Asseo (1993) as compared with this paper. Moreover, Asseo (1993) calculates the power emitted by soliton using a single-particle curvature radiation scheme, which is inapplicable as demonstrated in this paper (see eq.[12]).

A packet of plasma waves propagating through a relativistic electron-positron plasma with phase velocities close to the velocity of light is unstable from the modulation standpoint, and its nonlinear evolution results in the formation of a soliton. This process is described by a nonlinear Schrödinger equation with nonlinear Landau damping (Melikidze & Pataraya 1980b, 1984). In the case of electron-positron plasma the role of low-frequency perturbations is played by the nonlinear beatings of plasma waves, and the resonant interaction of beatings with particles determine the nonlinear damping.

In order to avoid confusion in the following discussion, we outline below the physics of the modulational instability occurring in the pulsar secondary pair plasma associated with sparking discharge of the polar gap. As already mentioned, the two-stream instability triggers linear plasma waves in electron-positron clouds created by succesive sparks. Obviously, there is a small spread $\Delta\omega$ of frequencies around the characteristic frequency ω_l (eq.[4]) of excited plasma waves. Since $\omega_l \gg \Delta\omega$, the amplitude of linear wave packet, containing waves with different frequencies near ω_l, will be modulated by low frequency beatings. The characteristic phase velocity of beatings $\Delta\omega/\Delta k$ is approximately equal to the group velocity of linear plasma waves $v_g = d\omega/dk$. Therefore, a resonant interactions of plasma particles with low frequency beatings (see the resonant factor $(v - v_g)^{-1}$ in eqs.[A8] - [A15]) will result in the modulational instability. Those low frequency beatings which are in resonance with plasma particles will affect the amplitude of linear waves in

the same way as the low frequency ion-sonic waves which affect the amplitude of Langmuir waves in the well-known laboratory electron-ion plasma (Zakharov & Shabat 1972).

In places where the amplitude of linear waves increase/decrease the plasma density n_p decreases/increases and, as a consequence, the characteristic frequency $\omega_l \propto (n_p)^{1/2}$ decreases/increases as well. On the other hand, the phase velocity of linear waves $v_f = \omega_l/k$ increases/decreases with increasing/decreasing frequency or with decreasing/increasing waves amplitude. Therefore, a spread of phase velocities along wave packet exists. Let us consider a point where the wave amplitude is a minimum and thus the phase velocity is a maximum at a given instant. The wave numbers change differently in different directions in the vicinity of this point. In fact, in the direction of waves propagation wavelengths λ will be shortened and in the opposite direction wavelengths will be lengthened. This means thats starting from the point of minimum amplitude, the wave numbers $k = 2\pi/\lambda$ increase in the direction of wave propagation and decrease in the opposite direction.

The behaviour of the modulationally unstable wave packet is determined by the so-called Lighthill condition (Lighthill 1967), which examines the sign of the product of coefficient G (describes dispersion; eq. [A5]) and q (describes grow of nonlinearity; eq. [A6]). If $Gq > 0$ then at places where the linear waves amplitude is near maximum, it will grow even larger. This should lead to self-condensation of the wave packet or soliton formation. Inspection of Figure 1 shows that in pulsar magnetospheres both G and q are positive in wide range of parameters (see eq.[A20] and Appendix C for definitions) and thus we can adopt that $Gq > 0$ in radio pulsars.

Let us check what effect the positive value of $G \propto dv_g/dk$ (eq.[A5]) has on the system of linear plasma waves in the vicinity of the point with minimum wave amplitude. Recall that wave numbers increase on one side (in the direction of propagation) and decrease on the other side of this point. Since $G > 0$, the group velocity v_g increases/decreases with increasing/decreasing wave number k. This means that energy of plasma waves flows out of the minimum amplitude region in both directions towards regions of higher and higher amplitudes. As a result, the energy of plasma waves gets packed into small regions where the amplitude grows even larger and the plasma density decreases, forming a low density cavities. The effective force which sweeps plasma particles out of the cavity is called ponderomotive force or the Miller force (Gaponov & Miller 1958), is just a measure of difference of the high-frequency electromagnetic pressure between regions of high and low amplitudes of plasma waves. This force is sensitive to mass and charge but insensitive to the sign of charge of plasma particles. In the laboratory plasma the ponderomotive force causes the effective charge separation due to huge difference in the inertia of ions and electrons (e.g. Sagdeev 1979). There have been many laboratory experiments confirming existence of the Miller force in an electron-ion plasma (see also Petviashvili 1976, for evidence of charge separation in the Earth ionosphere).
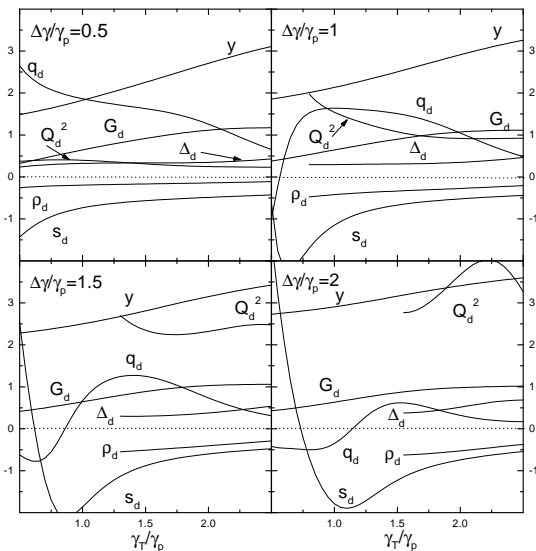
Fig. 1.— Values of different parameters (see Appendix C for explanations and definitions) versus thermal spread defined as γ_T/γ_p, where $\gamma_T \sim p_T$ is a Lorentz factor describing a degree of plasma thermalization and γ_p is average Lorentz factor of ambient plasma particles, for four different values of relative shift of electron and positron distribution functions $\Delta\gamma/\gamma_p = 0.5, 1.0, 1.5, 2.0$, respectively.

Let us then examine an influence of the Miller force on the electron-positron pair plasma. If the distributions of electrons and positrons are identical, then the Miller force affects electrons and positrons in the same rate, and effective charge separation will not occur. This can be directly noticed from equation (A19). However, in the pulsar magnetospheric plasma $f_e \neq f_p$. As demonstrated by Cheng & Ruderman (1977a) the difference between f_e and f_p is a result of variation of the product $\mathbf{\Omega} \cdot \mathbf{B}(\mathbf{r})$ along a flux tube of dipolar magnetic field lines. Since the numbers of electrons and positrons are equal, therefore the difference is in the average Lorentz factors of pair plasma components. One can show that $\Delta\gamma/\gamma_p \simeq \Delta\sigma\gamma_p^3/\gamma_b$ (e.g. Asseo & Melikidze 1998), where $\Delta\gamma$ is the difference of average Lorentz factors of electrons and positrons, and $\Delta\sigma = \sigma/\sigma_0 - 1$ is the normalised difference of the opening angles $\sigma = \arccos(\mathbf{\Omega} \cdot \mathbf{B}(\mathbf{r})/(\Omega B))$ between the point under consideration (σ) and the stellar surface (σ_0) along a given dipolar field line (see Appendix C for definitions of γ_p and γ_b). For a typical pulsar at altitudes of about 50 stellar radii $\delta\sigma \sim 0.5$. Thus for canonical values of Lorentz factors $\gamma_p \sim 100$ and $\gamma_b \sim 10^6$ we have $\Delta\gamma/\gamma_p \sim 0.5$, which is just enough to cause significant charge separation due to effective relativistic mass difference between electrons and positrons (see Fig. 1 for the parameter Q_d appearing in eq.[18]). If the surface magnetic field is non-dipolar, then $\Delta\gamma/\gamma_p$ can be even larger.

If a difference between the electron and positron distribution functions is small (that is $\Delta\gamma/\gamma \sim 1$), the dispersion of linear waves and the coefficients of the nonlinear Schrödinger equation remain almost unchanged with respect to the well-known case for which $\Delta\gamma = 0$ (Melikidze & Pataraya 1980a, 1984). Full details of derivation of the nonlinear Schrödinger equation for electrostatic waves in the relativistic electron-positron plasma associated with succession of spark-generated clouds are presented in the Appendix A. Below we outline the main results and discuss their implications for effective mechanism of pulsar radio emission.
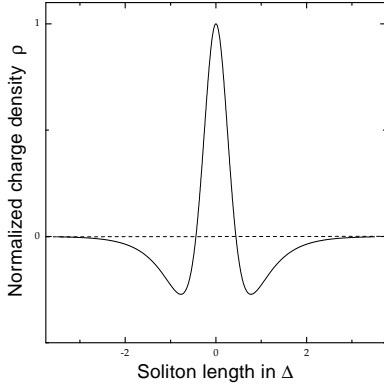

Fig. 2.— Normalized charge density ρ (eq.[8]) versus length in units of Δ (eq.[10]) of a spark-associated soliton (see Fig. 3 for the model of charge distribution).

As argued above, the soliton charge separation due to relative motion of electrons and positrons is supported by the pondemotorive or so called the Miller force (Gaponov & Miller 1958). In the LFR (Appendix A) the value of the charge density contrast associated with solitons can be determined by means of evaluating integrals in (A19) and substituting into it equation (A18). The expression for slowly varying charge density inside the soliton has the form

$$\rho \sim n_p \, e \, \chi^2 \, \frac{\cosh^2 \zeta - 2}{\cosh^3 \zeta} \rho_d \qquad \mathrm{cm}^{-\frac{3}{2}} \, \mathrm{g}^{\frac{1}{2}} \, \mathrm{s}^{-1}, \tag{8}$$

where e is a fundamental charge, n_p is a number density of unperturbed ambient plasma, ρ_d is dimensionless parameter about ~ 0.3 (Fig.1),

$$\zeta = \frac{z - v_g t}{\Delta}, \tag{9}$$

χ is defined by equation (A23) as a ratio of Langmuir waves and plasma energy densities, and

$$\Delta \approx \gamma_0^{-1} \, K_m^{-1} \sim 36 \, \gamma_2^{0.5} \, \varkappa^{-0.5} \, R_{50}^{1.5} \Delta_d \, \chi^{-0.5} \, P^{0.25} \, \dot{P}_{-15}^{-0.25} \qquad \mathrm{cm} \tag{10}$$

is the characteristic soliton length scale, i.e. its longitudinal (along the magnetic field lines) dimension in LFR, where γ_0 is a Lorentz factor of relative motion of WFR and LFR (Appendix A),

K_m is the wave vector of low frequency perturbation (A17), and Δ_d is a dimensionless parameter shown in Figure 1. As one can see, the range of characteristic soliton dimension Δ is between 10 and 100 cm in the LFR, so they should be capable of emitting coherent curvature radiation at radio wavelengths.

Figure 2 presents schematically a charge distribution corresponding to equation (8). This kind of charge distribution can be modeled as a system of three charged bunches (Fig.3) coupled to each other and moving along the circular trajectory with a radius of curvature $r_c = \mathcal{R}$. The value of the central charge is Q, but the whole system is neutral as each of the two side charges has value equal to $-\frac{1}{2}Q$ (an estimate of Q will be given later in the paper). The ratio of the soliton charge density (8) and Goldreich-Julian charge density ρ_{GJ} can be estimated as

$$\frac{\rho}{\rho_{GJ}} \sim \varkappa \, \chi^2 \, \rho_d, \tag{11}$$

where $\varkappa \sim 10^4$, $\chi \sim 0.1$ (see discussion below eq.[A23]) and $\rho_d \sim 0.3$ (see Figure 1). Thus, the soliton charge density is about 10 times the Goldreich-Julian corotational value $\rho_{GJ} = en_{GJ}$ (eq.[2]) or about 10^{-3} of the secondary (Sturrock multiplicated) ambient plasma charge density n_p (see eq.[8]).
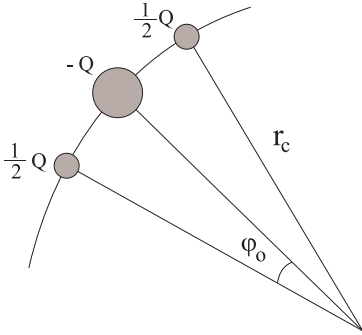

Fig. 3.— A simple model for the soliton with charge density shown in Fig. 2. The characteristic soliton length $\Delta = \varphi_o r_c$, where r_c is a local radius of curvature of the soliton trajectory.

Now let us examine the coherent curvature radiation of a centimeters long (in LFF) soliton bunches. The equation (B21) for the infinitesimal radiation intensity dI_n differs from the well-known equation for single particle curvature radiation intensity only by a term $[1 - \cos{(n\varphi_o)}]^2$, which does not depend on the solid angle σ. According to detailed calculations presented in Appendix B, the spectral power of our soliton is

$$I_\omega = \frac{Q^2}{c}\omega_0 F\left(\frac{\omega}{\omega_c}\right)\left[1 - \cos\left(a\frac{\omega}{\omega_c}\right)\right]^2 = \frac{Q^2}{c}\omega_0 F\left(\frac{\omega}{\omega_c}\right)\left[1 - \cos\left(\frac{2\pi}{c}\frac{\Delta}{\lambda}\right)\right]^2, \tag{12}$$

where $\omega_c = \frac{3}{2}\gamma_0^3\omega_0 \approx \gamma_0^3 c/\mathcal{R}$ is the characteristic frequency of single-particle curvature radiation, λ

is an emitted wavelength, the function

$$F(x) = x \int_x^\infty K_{\frac{5}{3}}(x) dx, \tag{13}$$

where $K_{\frac{5}{3}}(x)$ is the modified Bessel function and the parameter $a = \frac{\Delta}{\mathcal{R}} \gamma_0^3 \ll \frac{\pi}{2}$ (Appendix B) or

$$a \approx 8 \times 10^{-2} \, \gamma_2^{3.5} \, \varkappa_4^{-0.5} R_{50} \, y^3 \, \Delta_d \, \chi^{-0.5} \, P^{-0.25} \, \dot{P}_{-15}^{-0.25}. \tag{14}$$

Here $y = \gamma_0/\gamma_p$ is a dimensionless parameter describing the ratio of the Lorentz factors of solitons and bulk plasma particles in the radio emission region which is about unity for typical pulsar parameters.

To calculate the spectral power I_ω (eq.[12]) we have to find the soliton charge Q by integrating the charge density ρ (eq.[8]) over the soliton characteristic volume $\mathcal{V} \sim S_\perp \Delta$. Here $S_\perp$ is a soliton cross section, which we can estimate assuming that the perpendicular (with respect the magnetic field) size of the spark-associated plasma clouds at the stellar surface is about the gap height $h \simeq 5 \times 10^3 P^{3/7}$ cm (Paper I) and increases with a radial distance as r^3. Therefore

$$S_\perp \sim 3 \times 10^{12} \, R_{50}^3 \, P^{\frac{2}{7}} \, \dot{P}_{-15}^{-\frac{4}{7}} \qquad \text{cm}^2, \tag{15}$$

and

$$\mathcal{V} \sim 10^{14} \, \gamma_2^{0.5} \varkappa_4^{-0.5} \, R_{50}^{4.5} \, \Delta_d \, \chi^{-0.5} \, P^{0.54} \, \dot{P}_{-15}^{-0.82} \qquad \text{cm}^3, \tag{16}$$

which is about 10^{14} cm^3. Thus, a soliton charge $Q \simeq 10\rho_{GJ}\mathcal{V}$, where $\rho_{GJ} = en_{GJ} \sim e10^6$ cm^{-3} at the altitudes of about $50R$ (eq.[2]), which gives $Q \simeq e10^{21}$. Therefore,

$$I_\omega \sim 1.4 \times 10^{18} \gamma_2 \varkappa_4 R_{50}^{2.5} \chi^3 P^{-0.43} \dot{P}_{-15}^{-0.64} Q_d^2 \, F\left(\frac{\omega}{\omega_c}\right) \left[1 - \cos\left(a\frac{\omega}{\omega_c}\right)\right]^2 \quad \text{erg rad}^{-1}. \tag{17}$$

Consequently, the power radiated by one soliton $L_1 = \int I_\omega d\omega \simeq 4 \, \nu_c \, I_\nu$, where $\nu_c \sim \gamma_0^3 c/\mathcal{R}$ (see Fig.4) is the characteristic frequency of curvature radiation, is about

$$L_1 \sim 10^{22} \, \gamma_2^4 \, \varkappa_4 \, R_{50}^2 P^{-0.93} \, \dot{P}_{-15}^{-0.64} \left[\frac{y^3 \, \chi^3 \, Q_d^2 \, I_o(a)}{1.2 \times 10^{-4}}\right] \qquad \text{erg s}^{-1}, \tag{18}$$

where Q_d and $I_o(a) = \int F(x) \left[1 - \cos(ax)\right]^2 dx$ depend on the parameters of the plasma and their values for different cases are shown in Figures 1 and 5, respectively. This power is radiated mainly in the narrow frequency band around

$$\nu_m \sim 4.4 \times 10^7 \, \gamma_2^3 \, y^3 \, R_{50}^{-0.5} \, P^{-0.5} \qquad \text{Hz}, \tag{19}$$

which is about 4 times more than $\nu_c = \omega_c/2\pi$ (see Fig.4). Apparently, for $R_{50} \sim 2$, $\gamma_2 \sim 1$ and $y \sim 2.3$ this maximum frequency is close to 400 MHz, around which pulsars appear brightest.
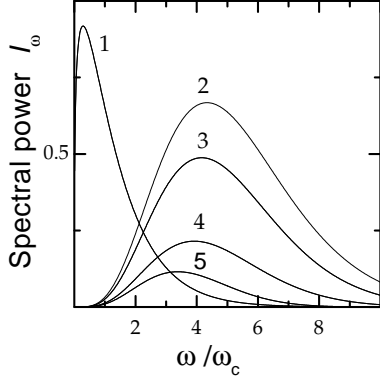
Fig. 4.— Normalized spectral power I_ω versus ω/ω_c, where ω is the frequency of curvature radiation and $\omega_c = 1.5\gamma_0^3 c/r_c$ (Appendix C) for: (1) single particle curvature radiation, and soliton curvature radiation with (2) $a = 0.1$, (3) $a = 0.2$, (4) $a = 0.3$ and (5) $a = 0.5$, where a is described in equation (14). The cases (1), (2), (3) and (4) are multiplied for clarity of presentation by a factor of 2000, 100, 10 and 1, respectively (see eqs.[12-18]) Notice that the frequency ν_m for which spectral power reaches maximum is about 4 times higher for solitons than for single particle curvature radiation.

The total number, N_t, of solitons contributing to pulsar radiation at any instant can be calculated as the number of sparks N_{sp} on the polar cap multiplied by the number of solitons N_{sl} associated with each spark. Since, as it is clear from figures 2 and 3, $N_{sl} \simeq \Delta r/(10\Delta)$, where $\Delta r \sim R_{50} \times 50R$ and Δ is a soliton length scale expressed in equation (10). Thus

$$N_{sl} \sim 1.4 \times 10^5 \; \gamma_2^{-0.5} \; \varkappa_4^{0.5} \; R_{50}^{-0.5} \; \Delta_d^{-1} \; \chi^{0.5} \; P^{-0.25} \; \dot{P}_{-15}^{0.25}. \tag{20}$$

The number of sparks on the polar cap with a radius $r_p \sim 10^4 P^{-0.5}$ cm is approximately equal to $(r_p/h)^2$, where r_p is the polar cap radius and $h \sim 5 \times 10^3 P^{3/7}$ cm is the polar gap height (for details see Paper I). Thus

$$N_{sp} \sim 25 \; P^{-1.3} \; \dot{P}_{-15}^{0.57} \tag{21}$$

and

$$N_t \sim N_{sp} \times N_{sl} \sim 3.5 \times 10^6 \; \gamma_2^{-0.5} \; \varkappa_4^{0.5} \; R_{50}^{-0.5} \; \Delta_d^{-1} \; \chi^{0.5} \; P^{-1.54} \; \dot{P}_{-15}^{0.82}. \tag{22}$$

Consequently, the total power $L_t = L_1 N_t$ radiated by a pulsar can be estimated as

$$L_t \sim 10^{28} \; \gamma_2^{3.5} \; \varkappa_4^{1.5} \; R_{50}^{1.5} P^{-2.47} \; \dot{P}_{-15}^{0.18} \left[6y^3 \; \chi^{3.5} \; Q_d^2 \; I_o(a) \, \Delta_d^{-1} \times 10^4 \right] \qquad \text{erg s}^{-1}. \tag{23}$$

Since the expression in square brackets is of the order of unity, it is clear from equation (23) that the power radiated by the spark-associated solitons can easily explain the observed radio emission of pulsars. In fact, for a typical pulsars the apparent luminosity is in the range $10^{25} - 10^{29}$ erg s^{-1} (see also Table 1).

3. Discussion

In this paper we propose a new, self-consistent theory of pulsar radio emission based on the modified non-stationary sparking model of Ruderman & Sutherland (1975). As argued by Gil & Sendyk in the accompanying Paper I, the polar cap with radius $r_p \sim 10^4 P^{-1/2}$ cm is populated with about $(r_p/h)^2$ sparks of a characteristic dimension approximately equal to the polar gap height $h \sim 5 \times 10^3 P^{3/7}$ cm. Each repeatable spark delivers to the open magnetosphere a sequence of $e^- e^+$ clouds, flowing orderly along dipolar magnetic field lines. Overlapping of particles with different momenta from consecutive sparks leads to a two-stream instability, which triggers a strong electrostatic Langmuir waves at the altitudes of about 50 stellar radii. This is the only known effective instability which can develop at low altitudes, where the narrow-band pulsar radiation originates (e.g., Kijak & Gil 1997, 1998). These oscillations with a characteristic frequency of about 100 GHz, are modulationally unstable and their nonlinear evolution results in the formation of 'bunch-like' charged solitons. A characteristic soliton length along the magnetic field lines is about 30 cm as viewed by a distant observer, so they are capable of emitting coherent curvature radiation at radio wavelengths. A perpendicular cross-section of each soliton at radiation altitudes results from a dipolar spread of a plasma clouds with a characteristic dimension of about $h \sim 50$ m near the neutron star surface. The net soliton charge Q is about 10^{21} fundamental charges e, contained within a volume of about 10^{14} cm^3. For a typical pulsar ($P \sim 1s, \dot{P} \sim 10^{-15}$), there are about 10^5 solitons associated with each of about 25 sparks operating on the polar cap at any instant. Since one soliton moving along dipolar field lines with a Lorentz factor γ of the order of 100 generates a power of about 10^{21} erg s^{-1}, then a total power of typical pulsar can be estimated as about 10^{27} erg s^{-1}. The degree of coherence for radio wavelengths is highest for smallest solitons. On the other hand, the net charge increases with the soliton size. This implies that the pulsar radiation should have a maximum intensity at some intermediate wavelength between 20 and 70 centimeters. This is really observed in most pulsars (e.g. Malofeev et al. 1994).

One of the reasons for such a huge net charge is that the soliton volume is large. Although only 30 cm in length along field line, it spans the entire transverse of the spark-associated plasma column. We make an implicit assumption that the soliton is transversely stable, at least over a time interval during which its curvature radiation is emitted towards an observer. Wheatherall (1997, 1998) has shown that an extremely strong plasma wave turbulence originating within the two-stream instability suffers rapid collapse transverse to the magnetic field. However, this effect is not relevant to our theory, since soliton amplitudes are limited by the non-linear Landau damping.

As far as millisecond pulsars are concerned, we cannot perform luminosity calculations for the following reason: the surface magnetic field inferred from P and $\dot{P}$ values is very small, typically $B_{12}^s \sim 10^{-4}$. This implies very large canonical gap height $h \sim 5 \times 10^3 \mathcal{R}_6^{2/7} B_{12}^{-4/7} P^{3/7}$ cm, typically close to 10^5 cm. Consequently, the spark-generated two-stream instability region would be located outside the light-cylinder and our theory can not be applied in the present form to the millisecond pulsars. However, it is quite possible that the surface field of millisecond pulsars is much stronger than the value inferred from the magnetic dipole braking law (see arguments by Cheng et al. 1998;

Cheng & Zhang 1999; Gil & Mitra 1999, and references therein). If this is the case, then everything scales properly and millisecond pulsars are not different from normal pulsars within the framework of our theory. We will present detailed intensity calculations for millisecond pulsars in a separate paper.

In our approach, contrary to those taken in previous studies, the problem of the formation of charged bunches is resolved automatically and self-consistently. The key feature of our picture is an existence of short-living ($\sim 10^{-5}$ s) sparks with both a characteristic dimension and typical distance between them equal approximately to the polar gap height $h \sim 5 \times 10^3 P^{2/7}$ cm (Paper I). As a result of their repeatable operation in approximately the same place, a two stream instability develops at low altitudes below 10% of the light cylinder radius, which generates high-frequency ($\nu \sim 100$ MHz) Langmuir electrostatic waves within the spark-associated plasma columns.

The soliton formation due to nonlinear development of strong Langmuir electrostatic waves is warranted by the hydrodynamical type of the linear instability, in which half of the energy of streaming charges can be transferred to the plasma turbulence. Because of the relative motion of centers of mass of electrons and positrons, the pondemotorive force acts on them differently, redistributing charges over the soliton volume. This results in a net soliton charge, consisting in fact from a system of three coupled localized charges. The soliton curvature radiation is much less effective than the curvature radiation of single small bunch with the same charge. However, since the soliton charge is huge, its curvature radiation is powerful enough to account for the observed pulsar radio emission. It is worth emphasizing that this radiation is supported by the kinetic energy of secondary $e^- e^+$ plasma with $\gamma_p \sim 100$, created via magnetic pair production by the primary beam with $\gamma_b \sim 10^6$ produced by the accelerating potential drop near the polar cap. It should be realized that a significant fraction of kinetic energy produced by sparks is radiated away in the form of soliton curvature radiation at radio wavelengths. In fact, the maximum kinetic luminosity associated with N_{sp} sparks (eq.[21]) is $L_m \simeq N_{sp} \dot{N}_s e f V$, where $\dot{N}_s \simeq 7 \times 10^{10} P_{-15}^{1/2} P^{-1/2} \pi h^2 c$ is the particle energy flux associated with a single spark. Here $1 > f > \mathcal{F}$, where $\mathcal{F} = 0.1 \mathcal{R}_6^{-5/21} B_{12}^{1/7} P^{1/7}$ is the filling factor (see Paper I) such that the actual accelerating potential of the developing spark is $\Delta V = f V$, where V is described by the maximum potential drop expressed in equation (1). Therefore, $L_m = 2.4 \times 10^{30} f \mathcal{R}_6^{8/7} B_{12}^{-9/7} \left(\dot{P}_{-15}/P \right)^{15/14}$ erg s^{-1}, and thus for $\mathcal{R}^{8/7} B_{12}^{-9/7} \sim 0.1$ and $f \sim 0.25$, we can write approximately

$$L_m \approx 5 \times 10^{28} \dot{P}_{-15} P^{-1} \ \text{erg s}^{-1}, \tag{24}$$

which is about an observable pulsar total radio luminosity.

In Table 1 we present results of the luminosity calculations from equation (23) for a number of pulsars with different values of period P and period derivative $\dot{P} = 10^{-15} \dot{P}_{-15}$. As one can see, it is easy to obtain the total luminosity L_t close to the observed luminosity $L_R \sim 3.5 \times 10^{25+x}$, where $x = \text{Log} (L)$ is taken from Table 4 in the pulsar catalog (Taylor et al. 1993), for a narrow range of parameters $\gamma_2 = \gamma_p/100$ and $y = \gamma_0/\gamma_p$ (Fig.1). This means that the pulsar luminosity $L_R \sim L_t$ is determined mainly by the values of P and $\dot{P}$, similarly to the morphological properties

of single pulses and average profiles (Paper I). The fraction $f = L_R/L_{sp}$, where $L_{sp} = 3.8 \times 10^{31} \dot{P}_{-15} P^{-3}$ erg/s is the pulsar spindown luminosity (Taylor et al. 1993), is a small number between $10^{-9} - 10^{-3}$, increasing towards longer periods, as observed. This is easy to understand bearing in mind that the soliton pulsar radiation is supported by the kinetic energy generated by the accelerating potential drop within the polar gap. In fact, if a significant fraction (say 30%) of spark maximum luminosity L_m (eqs.[23] and [24]) is converted to the soliton curvature radio emission, that is $L_R \sim L_t \sim 0.3\,L_m$, then $L_R/L_{sp} \sim 0.3 \times 10^{-4}\,P^2$. This ratio is about 3×10^{-8} for the Crab pulsar, 2×10^{-7} for Vela pulsar, 3×10^{-5} for one second pulsar, 4×10^{-4} for long period (3.75 s) pulsar and 2×10^{-3} for longest period (8.5 s) pulsar J2144-3933 (Young et al. 1999), in good agreement with data presented in Table 1.

In the framework of the soliton model presented in this paper, the frequency of radiated waves is much smaller than the characteristic frequency of the ambient plasma. For small angles between the wave vector and the external magnetic field, which is the case of the curvature radiation, spectra of these waves is $\omega = kc(1-\delta)$, where $\delta \propto \left(\omega_p/\omega_B\right)^2$ is negligibly small in the inner magnetosphere (e.g., Lominadze et al. 1986). Also Kazbegi et al. (1991) considered wave propagation in relativistic electron-positron pulsar magnetospheric plasma with $\Delta\gamma = \gamma_+ - \gamma_- \neq 0$ and showed that, in the case of propagation nearly along curved magnetic field lines there exist two elliptically polarised almost electromagnetic waves (with very small potential components). Therefore the curvature radiation at frequencies well below ω_l generated by relativistic soliton embedded in a surrounding plasma do have a dominating electromagnetic feature and can propagate through plasma, like in a vacuum.

Since the characteristic longitudinal dimension of our solitons is smaller than the emitted radio wavelengths, the polarization properties should be the same as in the case of single-particle curvature radiation modulated by the spark-associated envelope function (Gil & Snakowski 1990a), that is: (i) relatively high linear polarization with a position angle swing across the plane of the source motion and moderate circular polarization with sense reversals in the same plane (Michel 1987; Gil & Snakowski 1990b; Gil et al. 1993; Gangadhara 1997, 1999); (ii) the core components should differ from the conal components polarization-wise as a result of subpulse drift and/or scatter in conal parts of the mean profile (Gil et al. 1995; Paper I). In particular, the position angle in the core components should swing faster than predicted by the rotating vector model (Radhakrishnan & Cooke 1969), while in conal components the mean position angle curve should follow the rotating vector model more closely. On the other hand the circular polarization should typically change sense near the intensity maximum of core components, while in the conal components the circular position should be rather weak and mostly of one sense. All these specific properties are really observed (Rankin 1983; Lyne & Manchester 1988; Rankin 1990, 1993; Gil & Lyne 1995).

A. Nonlinear Schrödinger equation

The nonlinear Schrödinger equation is accepted as the fundamental equation to describe the nonlinear wave modulation in various kinds of the dispersive media (Karpman & Krushkal 1969; Taniuti & Yajima 1969; Zakharov & Shabat 1972). Usually when studying the nonlinear evolution of the Langmuir waves, the low frequency perturbation due to ion-acoustic waves is considered (e.g., Zakharov & Shabat 1972). But in the case of electron-positron plasma there is no such low frequency perturbation. An important effect associated with the resonance effects of particles moving at the group velocity was investigated by Ichikawa & Taniuti (1973) and they derived a nonlinear Schrödinger equation taking into account the nonlinear Landau damping. Contributions of the resonance particles at the group velocity of the wave modifies drastically the structure of the nonlinear Schrödinger equation in two respects. One is the appearance of a nonlocal-nonlinear term, which indeed arises from the nonlinear Landau damping process associated with the resonance at the group velocity of the wave. The other is the fact that the coupling coefficient of the local-nonlinear term is also modified by the contributions of these resonant particles. The relativistic case of this problem (when the plasma particle velocities are near the speed of light) was studied by Melikidze & Pataraya (1980a). They found that the resonant interaction between the nonlinear beatings and particles is of the primary importance in the case of electron-positron plasma (Melikidze & Pataraya 1980b).

Let us introduce two reference systems: the first system is connected with the neutron star and we will call it a *laboratory frame of reference* (LFR), the second one is moving with respect to the LFR with the velocity equal the group velocity of the of the Langmuir waves. We will call this system the *wave frame of reference* (WFR). We can study a one-dimensional case, which is correct for the pulsar magnetosphere as long as the magnetic field is strong enough to control the plasma motion. Let us assume that the external magnetic field is directed along the z-axis and that all perturbations are directed along the magnetic field. The z and time t-coordinates in the WFR is connected with LFR by the following formulas

$$z' = \gamma_0 \left(z - v_g t\right), \qquad t' = \gamma_0 \left(t - \frac{v_g}{c^2} z\right). \tag{A1}$$

Here $v_g = \partial \omega_l / \partial k_l$ is the group velocity of Langmuir waves and $\gamma_0 = \left(1 - v_g^2/c^2\right)^{-1/2}$. Thus, v_g and γ_0 are directly related with solitons propagating in an ambient secondary plasma with an average Lorentz factor γ_p (Table 1). In order to describe a nonlinear behavior of the wave packet we introduce the following representation of a distribution function and fields

$$F = F^{(0)} + \sum_{m=-\infty}^{\infty} \sum_{n=1}^{\infty} \varepsilon^n F_m^{(n)}(\xi, \tau) \exp\left(il\left(k_l' z' - \omega_l' t'\right)\right), \tag{A2}$$

where k_l' is a component of the wave vector along the magnetic field, ω_l' is the frequency of plasma waves in the WFR, ε is a small parameter of the perturbation theory and

$$\xi = \varepsilon z', \qquad \tau = \varepsilon^2 t'. \tag{A3}$$

This procedure separates slow and fast perturbations of plasma and wave parameters. Consequently, we are assuming that $\partial/\partial\tau \to \varepsilon^2$ and $\partial/\partial\xi \to \varepsilon$. To get a nonlinear Schrödinger equation it is sufficient and enough to derive a current of third order. Therefore we keep the sum in equation (A2) for values: $n = 1, 2, 3$ and $m = \pm1, \pm2, \pm3$. Substituting equations (A1 - A3) into the well-known kinetic Vlasov equation as well as satisfying the Maxwell equations, we obtain in the above approximation the so called nonlinear Schrödinger equation

$$i\frac{\partial}{\partial\tau}E_\parallel^{(1)} + G\frac{\partial^2}{\partial\xi^2}E_\parallel^{(1)} + q\left|E_\parallel^{(1)}\right|^2 E_\parallel^{(1)} + s\frac{1}{\pi}\oint\frac{\left|E_\parallel^{(1)}(\xi',\tau)\right|^2}{\xi - \xi'}d\xi' E_\parallel^{(1)} = 0. \qquad (A4)$$

This equation is written in the WFR, but of course the electric field $E_\parallel^{(1)}$ does not change when the frames are moving along the z-axis. The coefficients of the equation (A4) are following:

$$G = \frac{1}{2}\frac{d^2\omega_l'}{dk_l'^2} = \frac{1}{2}\gamma_0^3\frac{d^2\omega_l}{dk_l^2}, \qquad (A5)$$

$$q = -\frac{(\omega_l - k_l v_g)}{2k_l}\left\{\left(\frac{A^2}{6k_l} + \frac{B}{2}\right) - k_l\left(\frac{(W^2 - V^2)H + 2WVU}{H^2 - V^2} + C\right)\right\}, \qquad (A6)$$

$$s = \frac{(\omega_l - k_l v_g)}{2k_l}\left(\frac{(W^2 - V^2)U - 2WVH}{H^2 + V^2} + D\right), \qquad (A7)$$

where

$$W = \sum_\alpha \omega_{p\alpha}^2 \oint \frac{1}{(\omega_l - k_l v)^2}\frac{dv}{dp}\frac{1}{(v - v_g)}\frac{df_\alpha}{dp}dp \quad, \qquad (A8)$$

$$V = \sum_\alpha \omega_{p\alpha}^2 \int \frac{1}{(\omega_l - k_l v)^2}\frac{dv}{dp}\frac{df_\alpha}{dp}\delta(v - v_g)\,dp \quad, \qquad (A9)$$

$$A = \sum_\alpha \omega_{p\alpha}^2 \int \frac{1}{(\omega_l - k_l v)}\frac{d}{dp}\left(\frac{1}{(\omega_l - k_l v)}\frac{df_\alpha}{dp}\right)dp \quad, \qquad (A10)$$

$$B = \sum_\alpha e_\alpha\omega_{p\alpha}^2 \int \frac{1}{(\omega_l - k_l v)}\frac{d}{dp}\left\{\frac{1}{(\omega_l - k_l v)}\frac{d}{dp}\left(\frac{1}{(\omega_l - k_l v)}\frac{df_\alpha}{dp}\right)\right\}dp \quad, \qquad (A11)$$

$$C = -\sum_\alpha e_\alpha\omega_{p\alpha}^2 \oint \frac{1}{(\omega_l - k_l v)^2}\frac{dv}{dp}\frac{1}{(v - v_g)}\frac{d}{dp}\left(\frac{(v - v_g)}{(\omega_l - k_l v)^2}\frac{df_\alpha}{dp}\right)dp \quad, \qquad (A12)$$

$$D = \sum_\alpha e_\alpha\omega_{p\alpha}^2 \int \frac{1}{(\omega_l - k_l v)^2}\frac{dv}{dp}\delta(v - v_g)\frac{d}{dp}\left(\frac{(v - v_g)}{(\omega_l - k_l v)^2}\frac{df_\alpha}{dp}\right)dp \quad, \qquad (A13)$$

$$H = \sum_\alpha \omega_{p\alpha}^2 \oint \frac{1}{(v - v_g)}\frac{df_\alpha}{dp}dp \quad, \qquad (A14)$$

$$U = \sum_\alpha \omega_{p\alpha}^2 \int \delta(v - v_g)\frac{df_\alpha}{dp}dp \ . \qquad (A15)$$

Here α defines the sort of particles, ω_l, k_l and v are defined in the LFR. It should be mentioned that the equation (A4) is written in WFR, but all the values in the integrals are defined in LFR. In this paper we use dimensionless momentum normalized to $m_e c$.

Nonlinear evolution of the waves described by the equation (A4) is well known (e.g., Ichikawa et al. 1973). The maximum growth rate Γ_m of the modulational instability is defined as

$$\Gamma_m = \left(q^2 + s^2\right)^{\frac{1}{2}} \left|E_{\|o}^{(1)}\right|^2, \tag{A16}$$

and a corresponding wave vector of low frequency perturbation is

$$K_m = \left(\frac{q^2 + s^2}{Gq} \left|E_{\|o}^{(1)}\right|^2\right)^{\frac{1}{2}}. \tag{A17}$$

In the case when $|q| \gg |s|$ the equation (A4) has the following solution

$$E_{\|}^{(1)}(\xi, \tau) = E_{\|o}^{(1)} \operatorname{sech}\left(E_{\|o}^{(1)} \sqrt{\frac{q}{2G}} \left(\xi - u\tau\right)\right) \exp\left\{i\left(\frac{u}{2G}\xi - \frac{u^2}{4G}\tau + \frac{1}{2}q\tau\left(E_{\|o}^{(1)}\right)^2\right)\right\}. \tag{A18}$$

The slowly-varying charge density associated with developing soliton is given by the following formula

$$\rho' = \frac{\sum_\alpha e_\alpha \omega_{p\alpha}^2 \oint \frac{1}{(v-v_g)} \frac{d}{dp}\left(\frac{(v-v_g)}{\left(\omega_l - k_l v\right)^2} \frac{df_\alpha}{dp}\right) dp}{4\pi \sum_\alpha \omega_{p\alpha}^2 \oint \frac{1}{(v-v_g)} \frac{df_\alpha}{dp} dp} \times \frac{\partial^2}{\partial \xi^2} \mid E_{\|}^{(1)} \mid^2, \tag{A19}$$

where $E_{\|}^{(1)}$ is defined by the equation (A18). Let us note that this is a solution of the kinetic equation corresponding to the slowest mode only ($l = 0$ in eq.[A2]), thus describing a charge distribution within an envelope soliton. Since the distribution functions of electrons f_e and positrons f_p appearing in equation (A19) are not equal, the resulting charge density contrast associated with the soliton will be substantially non-zero.

It is known that if $qG > 0$ (the so-called Lighthill condition; Lighthill 1967), then the equation (A18) describes a soliton-like solution. For pulsar magnetospheric plasma the coefficients of equation (A4) are

$$\begin{aligned}
G &= \frac{1}{4}\frac{\gamma_p^2 c^2}{\omega_p}G_d, \\
q &= \left(\frac{e}{m_e c}\right)^2 \frac{1}{\gamma_p^2 \omega_p}q_d, \\
s &= \left(\frac{e}{m_e c}\right)^2 \frac{1}{\gamma_p^2 \omega_p}s_d,
\end{aligned} \tag{A20}$$

in the LFR, where G_d, q_d and s_d depend on the distribution function of plasma as shown in Figure 3. Obviously, the product $qG > 0$ for a wide range of parameters, so the Langmuir high

frequency oscillations modulated by the low-frequency beatings resulting from the range of linear wave frequencies, will evolve into the solitary waves. We are modelling the distribution function as

$$f_\alpha \sim \exp\left(-\left(\frac{p - p_\alpha}{p_T}\right)^2\right), \tag{A21}$$

where p_α for $p_e \approx \gamma_p$. In numerical calculations we are using $p_p/\gamma_p = (0.5 - 2)$, $p_T/\gamma_p = (0.5 - 1.5)$ and dimensionless momentum p_T describes a degree of plasma thermalization. The maximum growth rate of modulational instability can be written as

$$\Gamma_m \sim 2.7 \times 10^7 R_{50}^{-1.5} \left(\frac{\dot{P}_{-15}}{P}\right)^{0.25} \gamma_2^{-1.5} \left(q_d^2 + s_d^2\right)^{\frac{1}{2}} \chi, \tag{A22}$$

where

$$\chi \equiv \frac{\left|E_{\|o}^{(1)}\right|^2}{4\pi\gamma_p m_e c^2 n_o} \ll 1 \tag{A23}$$

which describes a ratio of energy densities of Langmuir waves and plasma. The nonlinear growth rate becomes equal to the linear one when $\chi \sim 0.04$. Typically $\chi \sim 0.1$, so the instability can easily develop with growth rate high enough to satisfy equation (7). The linear instability is of the hydrodynamical type, meaning that half of the particle's energy can be transferred to the plasma turbulence.

B. Coherent curvature radiation

In order to calculate a power of the coherent curvature radiation of the soliton modeled as a system of three coupled charged bunches presented in Figure 3, let us express the current in the form

$$\mathbf{J}(\mathbf{r}, t) = Q\left(\frac{d\mathbf{r}_0}{dt}\delta(\mathbf{r} - \mathbf{r}_0) - \frac{1}{2}\frac{d\mathbf{r}_1}{dt}\delta(\mathbf{r} - \mathbf{r}_1) - \frac{1}{2}\frac{d\mathbf{r}_2}{dt}\delta(\mathbf{r} - \mathbf{r}_2)\right), \tag{B1}$$

where $\mathbf{r}_0$ is the radius vector of the central bunch, and $\mathbf{r}_1$ and $\mathbf{r}_2$ are the radius vectors of the side bunches, respectively. The Cartesian components of radius vectors are

$$
\begin{aligned}
r_{0x} &= r_c \cos(\omega_o t), & r_{0y} &= r_c \sin(\omega_o t), \\
r_{1x} &= r_c \cos(\omega_o t + \varphi_o), & r_{1y} &= r_c \sin(\omega_o t + \varphi_o), \\
r_{2x} &= r_c \cos(\omega_o t - \varphi_o), & r_{2y} &= r_c \sin(\omega_o t - \varphi_o),
\end{aligned}
\tag{B2}
$$

where r_c is the radius of an effective circular orbit, $\varphi_o = \Delta/r_c$ is the angle between the central and peripheral particle's radius vectors, and $\omega_0 = v/r_c$ is the particles angular velocity (an effective gyro-frequency). The origin of the coordinate system is chosen in the center of the curvature, z-axis is directed perpendicular to the plane of the curvature, and y-axis is tangent and x-axis

is perpendicular to the local magnetic field, respectively. In our case $r_c = \mathcal{R}$ in the radiation generation region, where the radius of curvature of dipolar field lines

$$\mathcal{R} \sim 7 \times 10^8 R_{50}^{1.5} \ \text{cm}. \tag{B3}$$

According to a well-known method (e.g., Landau & Lifshitz 1962) we can calculate electromagnetic field of the charged system far from it, in the so-called 'wave zone'. Let us start with the standard determinations of the current Fourier components and vector potential. The current is

$$\mathbf{J}(\mathbf{r}, t) = \sum_{n=-\infty}^{\infty} \mathbf{J}_n(\mathbf{r}) e^{-i\omega_0 n t}, \tag{B4}$$

where

$$\mathbf{J}_n(\mathbf{r}) = \frac{1}{T} \int_{-T/2}^{T/2} \mathbf{J}(\mathbf{r}, t) e^{i\omega_0 n t} dt. \tag{B5}$$

The Fourier component of the vector-potential is defined as

$$\mathbf{A}_n = \frac{\exp(ikR_0)}{cR_0 T} \int_{-\infty}^{\infty} \int_{-T/2}^{T/2} \mathbf{J}(\mathbf{r}, t) e^{i(\omega_0 n t - \mathbf{k}\mathbf{r})} d\mathbf{r} dt, \tag{B6}$$

where R_0 is a distance from the radiating system to observer. In our case the current is just a motion of three small charged 'bunches'. The bunches are moving along the circular trajectory. In this configuration the central bunch has a charge Q and two other have the charge $-\frac{1}{2}Q$ each. This configuration is symmetric with respect of the central bunch. The axes are chosen as follows: The particles' trajectory lies in the plane $X0Y$, z-axis is perpendicular of this plane. $\mathbf{k}$-vector lies in the plane $Z0Y$. Consequently from equations (B1) and (B6) we obtain

$$\mathbf{A}_n = Q\frac{\exp(ikR_0)}{cR_0 T} \int_{-T/2}^{T/2} \left(\frac{d\mathbf{r}_0}{dt} e^{i(\omega_0 n t - \mathbf{k}\mathbf{r}_0)} - \frac{1}{2}\frac{d\mathbf{r}_1}{dt} e^{i(\omega_0 n t - \mathbf{k}\mathbf{r}_1)} - \frac{1}{2}\frac{d\mathbf{r}_2}{dt} e^{i(\omega_0 n t - \mathbf{k}\mathbf{r}_2)} \right) dt, \tag{B7}$$

where

$$\mathbf{k}\mathbf{r}_0 = kr_c \cos(\theta) \sin(\omega_0 t) ; \ \mathbf{k}\mathbf{r}_1 = kr_c \cos(\theta) \sin(\omega_0 t + \varphi_o) ; \ \mathbf{k}\mathbf{r}_2 = kr_c \cos(\theta) \sin(\omega_0 t - \varphi_o). \tag{B8}$$

Here θ is the angle between the $\mathbf{k}$-vector and y-axis, $T = 2\pi/\omega_0$, and we assume that $v \sim c$. Therefore, we have from equation (B7) for x and y components

$$\begin{aligned}
\mathbf{A}_{xn} &= -Qr_c\omega_0 \frac{\exp(ikR_0)}{cR_0 T} \int_{-T/2}^{T/2} \{\sin(\omega_0 t) \exp[i\omega_0 n t - ikr_c \cos(\theta) \sin(\omega_0 t)] - \\
&\quad -\frac{1}{2}\sin(\omega_0 t + \varphi_o) \exp[i\omega_0 n t - ikr_c \cos(\theta) \sin(\omega_0 t + \varphi_o)] - \\
&\quad -\frac{1}{2}\sin(\omega_0 t - \varphi_o) \exp[i\omega_0 n t - ikr_c \cos(\theta) \sin(\omega_0 t - \varphi_o)]\} dt.
\end{aligned} \tag{B9}$$

$$\mathbf{A}_{yn} \;=\; Qr_c\omega_0 \frac{\exp{(ikR_0)}}{cR_0T} \int\limits_{-T/2}^{T/2} \{\cos{(\omega_0 t)}\exp{[i\omega_0 nt - ikr_c\cos(\theta)\sin{(\omega_0 t)}]} -$$

$$-\frac{1}{2}\cos{(\omega_0 t + \varphi_o)}\exp{[i\omega_0 nt - ikr_c\cos(\theta)\sin{(\omega_0 t + \varphi_o)}]} -$$

$$-\frac{1}{2}\cos{(\omega_0 t - \varphi_o)}\exp{[i\omega_0 nt - ikr_c\cos(\theta)\sin{(\omega_0 t - \varphi_o)}]}\}dt. \tag{B10}$$

Introducing the following variables

$$\varphi = \omega_0 t, \qquad z = kr_c\cos(\theta) \tag{B11}$$

and using

$$\int\limits_{-\pi}^{\pi} \{\sin{(\varphi \pm \varphi_o)}\exp{[in\varphi - iz\sin{(\varphi \pm \varphi_o)}]}\}\,d\varphi = 2\pi i\exp{(\mp in\varphi_o)}\,J_n'(z)\,; \tag{B12}$$

$$\int\limits_{-\pi}^{\pi} \{\cos{(\varphi \pm \varphi_o)}\exp{[in\varphi - iz\sin{(\varphi \pm \varphi_o)}]}\}\,d\varphi = 2\pi\exp{(\mp in\varphi_o)}\,\frac{n}{z}J_n(z)\,, \tag{B13}$$

we obtain the components of the vector potential in the form

$$\mathbf{A}_{xn} = -2\pi i\left(Qr_c\frac{\exp{(ikR_0)}}{cR_0T}\right)[1 - \cos{(n\varphi_o)}]\,J_n'(z)\,; \tag{B14}$$

$$\mathbf{A}_{yn} = 2\pi\left(Qr_c\frac{\exp{(ikR_0)}}{cR_0T}\right)[1 - \cos{(n\varphi_o)}]\,\frac{n}{z}J_n(z)\,, \tag{B15}$$

where $J_n(z)$ is the Bessel function of the first order. For the radiation intensity with frequency $\omega = n\omega_0$ emitted within the solid angle $d\sigma$ we have

$$dI_n = \frac{c}{2\pi}\,|\mathbf{k} \times \mathbf{A}_n|^2\,R_0^2 d\sigma, \tag{B16}$$

where

$$|\mathbf{k} \times \mathbf{A}|^2 = A_x^2 k^2 + A_y^2 k^2 \sin^2{(\theta)}. \tag{B17}$$

So finally we obtain

$$dI_n \;=\; \frac{c}{2\pi}\left[A_{xn}^2 k^2 + A_{yn}^2 k^2 \sin^2{(\theta)}\right]R_0^2 d\sigma =$$

$$=\; 2\pi ck^2\left(\frac{Qr_c}{cT}\right)^2 [1 - \cos{(n\varphi_o)}]^2\left(J_n'(z)^2 + \frac{n^2}{z^2}J_n(z)^2\sin^2{(\theta)}\right)d\sigma. \tag{B18}$$

Taking into account that $\omega_0 = v/r_c$, $T = 2\pi/\omega_0$ and $kc = n\omega_0$, we find

$$dI_n = \frac{n^2 c}{2\pi r_c^2}Q^2\,[1 - \cos{(n\varphi_o)}]^2\left\{J_n'(z)^2 + \left(\frac{n}{z}\right)^2 J_n(z)^2\sin^2{(\theta)}\right\}d\sigma. \tag{B19}$$

Using $v \sim c$ and writing

$$\frac{n}{z} = \frac{n}{kr_c \cos(\theta)} \approx \frac{1}{\cos(\theta)}, \tag{B20}$$

where we make the approximation $z = kr_c \cos(\theta) \approx n \cos(\theta)$, we obtain

$$dI_n = Q^2 \frac{n^2 \omega_0^2}{2\pi c} [1 - \cos(n\varphi_o)]^2 \left\{ J_n'(z)^2 + \tan^2(\theta) J_n(z)^2 \right\} d\sigma. \tag{B21}$$

Since the part of the above equation in the square brackets does not depend on the solid angle σ and the integral of the part in the braces is well known in the relativistic case (Landau & Lifshitz 1962), the integral of (B21) is straightforward. Using $\omega = kc$, $I_\omega = I_n dn = I_n d\omega/\omega_0$, and

$$n\varphi_o = \frac{\omega}{\omega_0} \frac{\Delta}{r_c} = \frac{3}{2} \gamma_o^3 \frac{\Delta}{\mathcal{R}} \frac{\omega}{\omega_c} = a \frac{\omega}{\omega_c}, \tag{B22}$$

where $a = \gamma_0^3 \Delta/\mathcal{R}$ and φ_0 is marked in Figure 3, we can integrate expression (B21) which leads to equation (12) in the main body of the paper describing a spectral power emitted by solitons. From the condition for coherency $\Delta \ll \lambda/2$, where $\lambda \sim \pi\mathcal{R}/\gamma_0^3$ is a wavelength of the coherent radiation emitted by a soliton with characteristic size Δ, it follows that $a \ll \pi/2$.
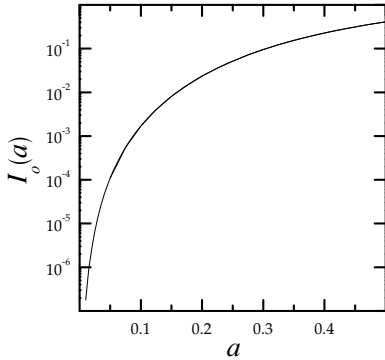

Fig. 5.— Values of the integral $I_o(a)$ (eq.[18]) versus parameter a (eq.[14]).

C. Definitions

$a = \gamma_0^3 \Delta/\mathcal{R}$ - dimensionless parameter (see eq.[14]).
$B_{12} = B_0/10^{12}$ G - value of the surface magnetic field in units of 10^{12} Gauss.
D - characteristic perpendicular spark dimension in cm (approximately equal to h).
Δ - characteristic soliton size along dipolar field lines (see eq.[10]).
Δ_d - dimensionless parameter shown in Figure 1.

$\Delta\gamma$ - difference between the average Lorentz factors of electrons and positrons.

$\delta_\omega \sim 0.5$ - dimensionless parameter calculated in Asseo & Melikidze (1998).

f_α - distribution function of type α plasma particles (see eq.[A21]).

G - cefficient of equation A4 (see eq.[A5]).

G_d - dimensionless parameter shown in Figure 1 (eq.[A20]).

Γ_l - linear growth rate (see eq.[6]).

Γ_m - growth rate of modulational instability (see eq.[A16]).

$\gamma_0 = (1 - v_g^2/c^2)^{-1/2}$ - Lorentz factor corresponding to solitons (see eq.[A1]).

$\gamma_b \sim 10^6$ - average Lorentz factor of the primary beam particles (see eq.[1]).

$\gamma_p \sim 100$ - average Lorentz factor of the plasma particles.

$\gamma_2 = \gamma_p/100$.

$\gamma_T \sim p_T$ - characteristic thermal spread of the plasma particles (eq.[A21]).

$h \simeq 5 \times 10^3 \; \mathcal{R}_6^{2/7} \; B_{12}^{-4/7} \; P^{3/7}$ cm - polar gap height.

I_ω - spectral power of coherent curvature radiation of a soliton (see eq.[17]).

$\varkappa \sim \gamma_b/\gamma_p$ - Sturrock's multiplication factor (for typical pulsar $\varkappa \sim 10^4$).

$\varkappa_4 = \varkappa/10^4$, $\varkappa_4 \sim 1.6/\gamma_2$ (see eq.[1]).

L_1 - power radiated by a single soliton (see eq.[18]).

L_m - maximum kinetic spark luminosity (see eq.[24])

L_{sd} - pulsar spin-down luminosity.

L_t - total power radiated by all solitons (see eq.[23]).

N_{sl} - number of solitons associated with a single spark (see eq.[20]).

N_{sp} - number of sparks on the polar cap (see eq.[21]).

N_t - total number of solitons (see eq.[22]).

ν_m - characteristic (maximum) frequency of the soliton curvature radiation (see eq.[19]).

$\omega_o = v/r_c$ - angular velocity of a particle.

$\omega_c = 1.5 \; \omega_o \gamma_0^3$ - characteristic frequency of single particle curvature radiation.

$\omega_l \simeq 2\delta_\omega \gamma_p \omega_p$ - characteristic frequency of the excited Langmuir waves (see eq.[4]).

$\omega_p = \left(4\pi e^2 n/m_e\right)^{1/2}$ - plasma frequency (see eq.[3]).

P - pulsar period in seconds.

$\dot{P}_{-15}$ - period derivative in units of 10^{-15} s s^{-1}.

Q - charge of the central bunch in the soliton wavelet (see Fig.3).

Q_d - dimensionless parameter shown in Figure 1.

q - coefficient of local-nonlinear term in equation A4 (see eq.[A6]).

q_d - dimensionless parameter shown in Figure 1 (see eq.[A20]).

$R_{50} = r/(50R)$ - distance from the stellar surface in 50 stellar radii $R = 10^6$ cm.

$\mathcal{R} \sim 7 \times 10^8 R_{50}^{1.5}$ cm - curvature radius of the dipolar magnetic field lines.

$\mathcal{R}_6 = \mathcal{R}/R$ - curvature radius of the magnetic field lines at the polar cap region in units of 10^6 cm.

r - radial coordinate (absolute value of radius vector).

$r_c \sim \mathcal{R}$ - curvature radius of particles trajectory.

$r_{in} \simeq R_{50} R$ - linear instability altitude.

$r_p \sim 10^4 P^{-0.5}$ cm - polar cap radius.

Δr - characteristic longitudinal dimension of linear instability region.

ρ - slowly-varying charge density inside soliton (see eq.[8]).

ρ_d - dimensionless parameter shown in Figure 1.

$S_\perp$ - cross-section of spark-associated soliton (see eq.[15]).

s - coefficient of non-local nonlinear term in equation A4 (eq.[A7]).

s_d - dimensionless parameter shown in Figure 1 (eq.[A20]).

V - canonical maximum potential drop within the gap in Volts.

$\mathcal{V}$ - volume of spark-associated soliton (see eq.[16]).

$v_g = \partial \omega_l / \partial k_l$ - group velocity of Langmuir waves in LFR.

$y = \gamma_0 / \gamma_p$ - dimensionless parameter shown in Figure 1.

REFERENCES

Asseo, E. 1993, MNRAS, 264, 940

Asseo, E., & Melikidze, G. I. 1998, MNRAS, 301, 59

Blaskiewicz, M., Cordes, J. M., & Waserman, I. 1991, ApJ, 370, 643

Cheng, K. S., Gil, J., Zhang, L. 1998, ApJ, 493, L35

Cheng, K. S., Zhang, L. 1999, ApJ, 515, 337

Cheng, A. F., & Ruderman, M. A. 1977a, ApJ, 212, 800

Cheng, A. F. & Ruderman, M. A. 1977b, ApJ, 214, 598

Cheng, A. F. & Ruderman, M. A. 1980, ApJ, 235, 576

Cordes, J. M. 1978, ApJ, 222, 1006

Cordes, J. M. 1992, in IAU Colloq. 128, The Magnetospheric Structure and Emission Mechanism of Radio Pulsars, ed. T. H. Hankins, et al. (Zielona Góra, Poland: Pedagogical Univ. Press), 253

Deshpande, A. A., & Rankin, J. M. 1999, ApJ, 524, 1008

Gangadhara, R. T. 1997, A&A, 327, 155

Gangadhara, R. T. 1999, A&A, 392, 474

Gaponov, A. V., & Miller, M. A. 1958, Soviet Phys. JETP, 34, 242

Gil, J., Kijak, J., Maron, O., & Sendyk, M. 1995, A&A, 301, 177

Gil, J., Kijak, J., & Zycki, P. 1993, A&A, 272, 207

Gil, J., & Lyne, A.G., 1995, MNRAS, 276, L55

Gil, J., Krawczyk, A., & Melikidze, G. I. 1997, Banach Center Publications, vol.41/2, (Warsaw: Polish Academy of Sciences), 239

Gil, J., & Mitra, D. 1999, A&A, submitted

Gil, J., & Sendyk, M. 2000, ApJ(Paper I)

Gil, J., & Snakowski, J. K. 1990a, A&A, 234, 237

Gil, J., & Snakowski, J. K. 1990b, A&A, 234, 269

Goldreich, P., & Julian, H. 1969, ApJ, 157, 869

Ichikawa, Y. H., & Taniuti, T. 1973 J. Phys. Soc. Japan, 34, 513

Ichikawa, Y. H., Suzuki, T., & Taniuti, T. 1973, J. Phys. Soc. Japan, 34, 1089

Karpman, V. I., Norman, C.A., ter Haar, D., & Tsitovich, V. N. 1975, Phys. Scripta, 11, 271

Karpman, V. I., & Krushkal, E. M. 1969, JETP, 28, 277

Kazbegi, A.Z., Machabeli, G.Z., & Melikidze, G.I. 1991, MNRAS, 253, 377

Kazbegi, A. Z., Machabeli, G. Z., & Melikidze, G. I. 1992, in IAU Colloq. 128, The Magnetospheric Structure and Emission Mechanism of Radio Pulsars, ed. T. H. Hankins, et al. (Zielona Góra, Poland: Pedagogical Univ. Press), 232

Kijak, J., & Gil, J. 1997, MNRAS, 288, 631

Kijak, J., & Gil, J. 1998, MNRAS, 299, 855

Landau, L. D., & Lifshitz, E. M. 1962, Classical Theory of Fields (Oxford: Pergamon Press)

Lighthill, M. J. 1967, Proc. Roy. Soc. A229, 28

Lominadze, J. G., Machabeli, G. Z., Melikidze, G. I., & Pataraya, A. D. 1986, Sov. J. Plasma Phys., 12, 712

Lutikov, M., Blandford, R. D., & Machabeli, G. 1999, MNRAS, 305, 338

Lyne, A. G., & Manchester, R. N. 1988, MNRAS, 234, 477

Machabeli, G. Z. 1991, Plasma Phys. and Controlled Fusion, 33, 1227

Malofeev, V. M., Gil, J., Jessner A., Malov, I., Sieber, W., & Wielebinski, R. 1994, A&A, 285, 201

Melikidze, G. I., & Pataraya, A. D. 1980, Ap&SS, 68, 49

Melikidze, G. I., & Pataraya, A. D. 1980, Astrofizika, 16, 161

Melikidze, G. I., & Pataraya, A. D. 1984, Astrofizika, 20, 157

Melrose, D. B., & Gedalin, M. E. 1999, ApJ, 521, 351

Michel, F. C. 1987, ApJ, 322, 822

Petviashvili, V.I. 1976, Sov. J. Plasma Phys., 2, 247

Radhakrishnan V., & Cooke D. J. 1969, Astrophys. Lett., 3, 225

Rankin, J. M. 1983, ApJ, 274, 33

Rankin, J. M. 1990, ApJ, 352, 314

Rankin, J. M. 1993, ApJ, 405, 285

Ruderman, M. A., & Sutherland, P. G. 1975, ApJ, 196, 51

Sagdeev, R. Z. 1979, Rev. Mod. Phys., 51, 1

Sturrock, P. A. 1971, ApJ, 164, 529

Taylor, J. H., Manchester, R. N., & Lyne, A. G. 1993, ApJS, 88, 529 (Pulsar Catalog)

Taniuti, T., & Yajima, N. 1969, J. Math. Phys., 10,1369

Ursov, V. N., & Usov, V. V. 1988, Ap&SS, 140, 325

Usov, V. V. 1987, ApJ, 320, 333

Wheatherall, J.C. 1997, ApJ, 483, 402

Wheatherall, J.C. 1998, ApJ, 506, 341

Xu, R.X., Qiao, G.J., Zhang, B. 1999, ApJ, 522, L109

Young, M.D., Manchester, R.N., & Johnston, S. 1999, Nature, 400, 848

Zakharov, V. A., & Shabat, A. B. 1972, Soviet Phys. JETP, 34, 62

Table 1.   Observed and calculated pulsar luminosities.

PSR	P [s]	$\dot{P}_{-15}$	L_{sd} [erg/s]	L_R erg/s	L_t [erg/s]	y	γ_2
B0531+21	0.033	421	4.6×10^{38}	1.3×10^{29}	1.7×10^{29}	1.5	1
B0833−45	0.0893	125	6.9×10^{36}	4.3×10^{28}	8.0×10^{28}	1.6	1
B1610−50	0.232	493	1.6×10^{36}	2.8×10^{28}	7.7×10^{28}	2	1
B0950+08	0.253	0.229	5.6×10^{32}	2.3×10^{26}	6.6×10^{26}	1.5	0.65
B1133+16	1.188	3.73	8.8×10^{31}	7.4×10^{26}	9.6×10^{26}	2	0.9
B1746−30	0.61	7.9	1.4×10^{33}	3.0×10^{28}	9.4×10^{28}	2.2	1
B0525+21	3.75	40	3.0×10^{31}	1.1×10^{28}	1.5×10^{28}	2	1.2
J2144−39*	8.51	0.48	3.0×10^{28}	5.0×10^{24}	7.2×10^{24}	2.2	0.9

Note. — PSR name, P - pulsar period in seconds, $\dot{P}_{-15}$ - period derivative in 10^{-15}s s^{-1}, $L_{sd} = 3.8 \times 10^{31} \dot{P}_{-15} P^{-3}$ erg s^{-1} - spindown luminosity, $L_R = 3.5 \times 10^{25+x}$ erg s^{-1} - observed radio luminosity, where $x = \mathrm{L}og\, L$ in mJy kpc^2 from the pulsar catalog, L_t - total pulsar luminosity calculated from equation (23), parameters y and γ_2 used in calculations (see Appendix C and Figure 1 for explanations). $*$ - data for PSR $J2144 - 3933$ are taken from Young et al. (1999)